ISSN 1063-7826, Semiconductors, 2016, Vol. 50, No. 5, pp. 572–578. © Pleiades Publishing, Ltd., 2016.
Original Russian Text © V.V. Sobolev, D.A. Perevoshchikov, 2016, published in Fizika i Tekhnika Poluprovodnikov, 2016, Vol. 50, No. 5, pp. 582–588.

ELECTRONIC PROPERTIES OF SEMICONDUCTORS

Localization of the Interband Transitions in the Bulk of the Brillouin Zone of III–V Compound Crystals

V. V. Sobolev* and D. A. Perevoshchikov

Udmurt State University, Izhevsk, 426034 Russia

**e-mail: sobolev@uni.udm.ru*

Submitted September 17, 2015; accepted for publication October 14, 2015

Abstract—The localization of the transitions in the bulk of the Brillouin zone that form the main structures in the spectra of the imaginary part of the permittivity in the range up to ~7 eV for III–V semiconductors (AlSb, GaSb, InSb, and InAs) is determined using electron density functional theory. It is established that intense transitions occur not only in the vicinity of the high-symmetry axes of the Brillouin zone, but also in some specific large volumes of the irreducible part of the Brillouin zone.

DOI: 10.1134/S1063782616050213

1. INTRODUCTION

III–V Semiconductors are widely used for the fabrication of various optoelectronic devices [1]. Therefore, its electronic structure has been investigated in many experimental and theoretical studies [2–29]. The theoretical curves of the imaginary part of the permittivity $\varepsilon_2(E)$ [8–21] in the range to ~7 eV include three maxima (E_1, E_2, and E_1') and a wide step E_0' between E_1 and E_2. In rare cases [9, 11, 13, 14, 18, 20], a poorly pronounced structure is observed between E_2 and E_1', which has no commonly accepted notation and hereinafter is denoted as E_x.

The characteristic feature of these studies is that the $\varepsilon_2(E)$ spectral maxima are caused by transitions at high-symmetry points Γ, L, X, and K of the Brillouin zone (BZ) and along three axes Λ (Γ – L), Δ (Γ – X), and Σ (Γ – K); the irreducible part of the BZ is shown in Fig. 1. Hereinafter, the coordinates of all points in reciprocal space are given in the units $2\pi/a_0$, where a_0 is the crystal-lattice parameter, and the system of coordinates is chosen such that the coordinates of the BZ high-symmetry points acquire the values (0, 0, 0) for Γ, (0.5, 0.5, 0.5) for L, (1, 0, 0) for X, (0.75, 0.75, 0) for K, (1, 0.25, 0.25) for U, and (1, 0.5, 0) for W.

The maximum E_1 with the longest wavelength is formed by transitions from the two upper valence bands (UVBs) V_1 and V_2 to the lower conduction band (LCB) C_1 at the Λ axis. It is located in the portion from the point (0.15, 0.15, 0.15) to L, depending on the crystal and calculation technique [8–13, 18] or only in the immediate vicinity of point L [17, 19, 21]. The maximum E_2 is formed mainly by transitions between the UVB and LCB [8–14]. The most intense transitions occur in the vicinity of the Σ axis from the point (0.45, 0.45, 0) to the point K [8, 10–12], as well as along the Δ axis [8, 9, 11, 17, 19, 21], especially near the point X [8, 9, 17, 21]. The existence of the third maximum E_1' is attributed to transitions from the bands V_1 and V_2 to C_2 located at the point L [9, 10, 13, 21] and its vicinity to the point (0.375, 0.375, 0.375) [11, 12] and on the Δ axis [11]. The existence of the small structure E_x is related to transitions from the UVB to the second LCB (C_2) that occur in the bulk of the BZ near the points from ~(0.5, 0.0, 0.0) to ~(0.7, 0.0, 0.0) on the Δ axis [9, 11, 13, 14]. The step E_0' is formed with the involvement

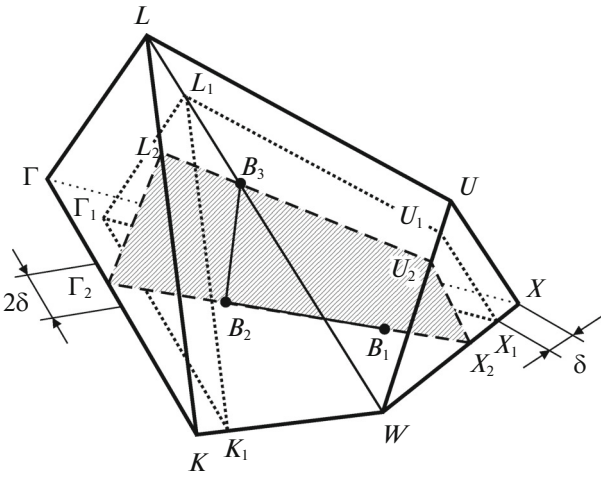

Fig. 1. Irreducible part of the Brillouin zone and schematic arrangement of the $\Gamma_1L_1U_1X_1$ and $\Gamma_2L_2U_2X_2$ planes and the points B_1, B_2, and B_3.

of transitions from two UVBs: in the LCB in the portion of the Δ axis from (0.5, 0.0, 0.0) to (0.7, 0.0, 0.0) [9, 11, 12, 18] and the second LCB in the vicinity of the BZ center [8, 9, 11, 13, 17, 18].

In addition, in [9, 10, 13, 18], quantitative schemes of the more complex localization of the transitions and their positioning in a wide range of **k** points were suggested. The largest differences in the schemes of localization of the transition structures occur in the case of the main maximum E_2. In particular, the decisive role in the formation of E_2 is played by the $X-U$ axis and its vicinity [9], the Δ, $W-K$, and $L-W$ axes [18], the vicinity of the point K and the $L-U$ axis of triangular shapes at the ΓLK and ΓLUX faces of the irreducible part of the BZ [10], and the vicinity of the point (0.75, 0.25, 0.25) at ΓLUX [13]. The bands E_x and E_1' in [18] are formed by transitions from V_1 and V_2 to C_2 along the Δ, $X-W$, and $L-W$ axes.

Thus, in all these calculations, the localization of the transition bands of four III–V crystals was investigated using only the general schemes of isoenergetic surfaces with very approximate indication of the region of their positioning in the BZ. It is commonly accepted that the role of a BZ region in the formation of $\varepsilon_2(E)$ spectral structures is a nontrivial problem; the data of different calculations are noticeably different and contradictory.

The optical spectra of the III–V crystals in a wide energy range were experimentally investigated in many studies [2–6, 24–27]. The permittivity spectra were obtained using ellipsometry techniques mainly in the range of 1.5–6.5 eV at temperatures of $T = 10$ K for GaSb [25], 22 K for InAs [27], 100 K for InSb [26], and 300 K for AlSb [24]. In all these spectra, one can clearly see the long-wavelength maximum E_1 at (2.4 ± 0.45) eV, the main maximum E_2 at (4.27 ± 0.27) eV, and the poorly pronounced maximum E_1' at higher energies. In addition, on both sides of the main maximum, there are structures E_0' and E_x with a lower intensity.

In [3, 5–7], III–V crystals were investigated in the region of the long-wavelength absorption edge at liquid-helium temperatures. This allowed their UVB and LCB in the vicinity of the point Γ to be investigated and the band gaps to be determined with high accuracy: GaSb, InSb, and InAs are direct-gap semiconductors with direct band gaps $E_{gd}^e(\Gamma) = 0.811$, 0.23, and 0.418 eV, respectively (the index e indicates experimental values). The AlSb UVB maximum is located at the center of the BZ, the LCB minimum, at the point X, and the corresponding value of the indirect band gap is $E_{gi}^e(\Gamma - X) = 1.677$ eV.

The aim of this study is to obtain new information on the localization of the transition bands for the four most popular III–V crystals in specific BZ volumes.

2. CALCULATION TECHNIQUE

The bands and spectra of the imaginary part of the permittivity of the four III–V compounds were calculated on the basis of electron-density functional theory using the Wien2k software package [30] without taking spin–orbit coupling into account. The spin-orbit interaction mainly splits the long-wavelength maximum E_1 into a doublet without changing its relatively simple localization and only slightly affects the other $\varepsilon_2(E)$ structures. Therefore, disregarding this effect noticeably simplifies the calculation without a decrease in the information supplied on the localization and energy of the other $\varepsilon_2(E)$ maxima. In this software package, the FP–LAPW technique is used and the generalized gradient approximation GGA–PBE is applied as an exchange–correlation potential [31]. The experimental lattice parameters of the crystals are $a_0 = 6.1355$ Å for AlSb, 6.096 Å for GaSb, 6.479 Å for InSb, and 6.058 Å for InAs [28]. The main drawback of ab initio calculations with the use of the local-field and generalized gradient approximations is a noticeable reduction in the band-gap energy $E_{gd}(\Gamma)$ [5, 20–23, 29]. This effect is especially pronounced in narrow-gap crystals with experimental values of $E_g(\Gamma) = 0.23$ (InSb) and 0.418 eV (InAs): when the experimental crystal-lattice parameter a_0 is used, the theoretical band gap E_{gd} vanishes. Therefore, without loss of generality of the calculated transition-band localization spectra, we obtained the positive energies $E_{gd}(\Gamma)$ for InSb and InAs in the calculation of their bands with use of the parameters $a_0 = 6.364$ and 5.900 Å decreased by 1.8–2.6% of their experimental values for InSb and InAs, respectively. Integration over the entire volume of the irreducible part of the BZ was performed by the tetrahedral technique [32] on the basis of 4612 K points. In calculating the spectra of the imaginary part of the permittivity, we used the formula [5]

$$\varepsilon_2 = \frac{4\pi^2 e^2}{m^2(\hbar\omega)^2\Omega_0}\sum_{V,C}\int_S \frac{|P_{CV}|^2 f(E_C)[1-f(E_V)]}{|\nabla_{\mathbf{k}}(E_C(\mathbf{k}) - E_V(\mathbf{k}))|}dS, \quad (1)$$

where e and m are the elementary charge and electron mass, respectively; Ω_0 is the unit-cell volume; E_V and E_C are the valence- and conduction-band energies, respectively; P_{CV} is the matrix element of the probability of the transition from the valence band V to the conduction band C; $f(E)$ is the Fermi–Dirac distribution function; and S is the surface of constant energy $E_C(\mathbf{k}) - E_V(\mathbf{k}) = \hbar\omega$. It can be seen that the $\varepsilon_2(E)$ spectrum has features at $\nabla_{\mathbf{k}}E_C = \nabla_{\mathbf{k}}E_V$, i.e., in the case of covariance of the valence and conduction bands. This underlies the highly simplified, yet frequently applied theoretical analysis of the ε_2 curves; the $\varepsilon_2(E)$ spectral maxima are assigned to the transitions with energies at which the corresponding pairs of bands are covariant in the largest region of **k** space. In addition, a noticeable role in the permittivity calculations can be played

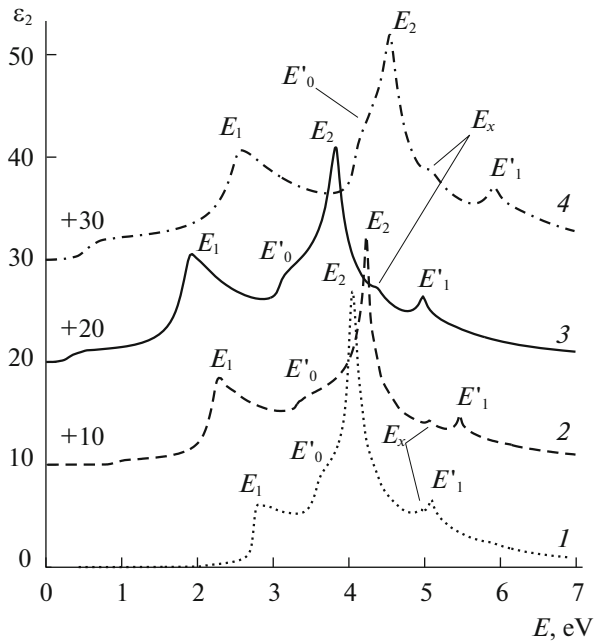

Fig. 2. Functions $\varepsilon_2(E)$ of the (*1*) AlSb, (*2*) GaSb, (*3*) InSb, and (*4*) InAs crystals.

by the matrix element of the transition probability P_{CV} in the light-wave electromagnetic field [33] determined from the formula

$$P_{CV} = -A_0 \frac{ie\hbar}{mc\Omega_0} \int_{\Omega_0} \psi^*_{V,\mathbf{k}}(r) \nabla \psi_{C,\mathbf{k}}(r) dr, \qquad (2)$$

where $\psi_{V,\mathbf{k}}$ and $\psi_{C,\mathbf{k}}$ are the initial and final electronic states, A_0 is the amplitude of the electromagnetic-wave vector potential, and c is the speed of light in vacuum. Taking into account P_{CV} can significantly change the interband transition intensity.

Based on the obtained data on the band structure and matrix elements of the transition probabilities, the localization of transitions in the BZ was determined using the software package developed at the Optical Spectroscopy Department of Udmurt State University. For the widest maxima E_1 and E_2, transition localization was studied not only for the maximum energy, but over the energy range where the majority of the investigated band is located.

3. RESULTS OF CALCULATIONS AND DISCUSSION

First, we calculated the energy bands of the AlSb, GaSb, InSb, and InAs crystals over the entire BZ volume. It was established that GaSb, InSb, and InAs are direct-band semiconductors with the band gap E^t_{gd} at the point Γ : $E^t_{gd}(\Gamma) = 0.33$ eV (GaSb), 0.11 eV (InSb), and 0.15 eV (InAs) (index t indicates that the values were obtained theoretically). The UVB maximum for AlSb is located at the point Γ; the LCB minimum is located at the point X; and the band-gap energies acquire values of $E^t_{gd}(\Gamma) = 1.61$ eV, $E^t_{gi}(\Gamma - L) = 1.37$ eV, and $E^t_{gi}(\Gamma - X) = 1.25$ eV. We introduce the corrections $\Delta_{e-t} = E^e_{gd}(\Gamma) - E^t_{gd}(\Gamma)$ for GaSb, InSb, and InAs and $\Delta_{e-t} = E^e_{gi}(\Gamma - X) - E^t_{gi}(\Gamma - X)$ for AlSb, which are related to the traditional reduction of the theoretical data on E^t_g relative to the experimental data on E^e_g. Thus, our calculated data are reduced by 0.12–0.48 eV: $\Delta_{e-t} = 0.43$ eV (AlSb), 0.48 eV (GaSb), 0.12 eV (InSb), and 0.27 eV (InAs).

The AlSb bands have no significant differences from the bands of the other investigated compounds, except for the indirect-gap character. Therefore, below we denote the bands of all four crystals similarly. The upper valence bands V_1 and V_2 are degenerate along the two principle axes, Λ and Δ, and in their closest proximity. At the other BZ high-symmetry points, the level V_2 is located lower than V_1 by an energy ranging from 0.5 to 1.5 eV. Assuming the traditional scheme of UVB maximum positioning at the point Γ to be an energy reference point, we obtain that the two UVBs in all the crystals are located in the range from 0 to (-3.5 ± 0.3) eV and the third UVBs lie in the range from 0 to (-6.2 ± 0.8) eV. The lower conduction bands have a complex structure and overlap in many directions. The width of the two lower conduction bands C_1 and C_2 are ~(4.3 ± 0.3) eV.

Then, based on the obtained bands with regard to the correction Δ_{e-t}, for each crystal the spectra of the imaginary part of the permittivity $\varepsilon_2(E)$ were calculated. They contain five main structures: E_1, E'_0, E_2, E_x, and E'_1 (Fig. 2). The energies of these structures are listed in Table 1 in comparison with similar values from other theoretical and experimental publications. The difference between our data and the experimental results is predominantly no larger than 0.1 eV and reaches 0.36 eV for E_2 (InSb) and E'_1 (InAs). It is worth noting that, due to the features of symmetry of the bands V_1 and V_2, the intensities of the transitions with their involvement are radically different. The vicinity of the long-wavelength maximum E_1 from the energy of the long-wavelength absorption edge to the step E'_0 forms the transitions from only two degenerate UVBs to the LCBs ($V_{1,2} \to C_1$). In the high-energy region (step E'_0), transitions to the second LCB ($V_{1,2} \to C_2$) begin. The most intense maximum E_2 is formed mainly by the transitions $V_1 \to C_1$ (see the second column in Table 2). Starting from E_x, their contribution, along with $V_2 \to C_1$, significantly decreases. Therefore, in the region of structures E_x and E'_0 the decisive role

Table 1. Energies of the main structures in the ε_2 spectra of the AlSb, GaSb, InSb, and InAs crystals

Compound	Source	E_1	E_0'	E_2	E_x	E_1'
AlSb	our data	2.81	3.73	4.05	4.95	5.09
	exptl. [24]	2.838	3.76	4.00	–	5.22
	theor. [15]	2.8	–	3.8	–	4.7
	theor. [17]	2.67	3.44	3.86	–	5.06
GaSb	our data	2.28	3.38	4.23	5.06	5.47
	exptl. [25]	2.16	3.4	4.13	5.11	5.4
	theor. [15]	1.9	–	3.6	–	4.8
	theor. [17]	1.95	3.04	4.00	–	–
InSb	our data	1.93	3.22	3.83	4.42	4.98
	exptl. [26]	1.968	3.14	4.186	–	5.22
	theor. [16]	2.17	–	4.10	–	5.20
	theor. [17]	1.86	2.88	4.13	–	5.09
InAs	our data	2.63	4.17	4.54	5.07	5.91
	exptl. [27]	2.608	–	4.54	5.282	6.261
	theor. [17]	2.55	4.21	4.61	–	–
	theor. [20]	3.33	–	4.55	5.10	5.90

All the values are given in eV, exptl., and theor. indicate experimental and theoretical results, respectively.

Table 2. Contributions (%) of the transitions $V_1 \to C_1$ of the $\varepsilon_2(E)$ spectrum to the intensity of the main E_2 maximum in different regions of the Brillouin zone of the AlSb, GaSb, InSb, and InAs crystals

Compound	Region				
	the entire Brillouin-zone volume	ΓLUX	$\Gamma_1 L_1 U_1 X_1$	region II	region III
AlSb	88.5	30	12	13	33.5
GaSb	92	39	12	7	34
InSb	86	29	16	3	37.5
InAs	84	31	15	7	31

is played by the transitions $V_1 \to C_2$. The effect of the other pairs of bands is weaker. Therefore, until ~7 eV, it is sufficient to consider localization in reciprocal space for only transitions from the two UVBs to the two LCBs. It should be taken into account that in describing our data on localization in any BZ region, we will also take into account its vicinity with radius δ, unless the other is specified ($\delta \approx 0.0434 \times 2\pi/\text{Å}$).

3.1. The E_1 Maximum

According to the calculations, transitions to the regions of the long-wavelength maximum occur only from the two UVBs to the LCB. The intensity of the transition $V_1 \to C_1$ is higher than the intensity of the transition $V_2 \to C_1$ by a factor of 2–2.5. Both bands are concentrated mainly in the following Λ axis segments: from L(0.5, 0.5, 0.5) to the point (0.15, 0.15, 0.15) and from L to the point (0.44, 0.44, 0.44) for AlSb; from L to the point (0.24, 0.24, 0.24) and from the point (0.22, 0.22, 0.22) to the point (0.15, 0.15, 0.15) for GaSb; from the point (0.41, 0.41, 0.41) to the point (0.22, 0.22, 0.22) and from L to the point (0.26, 0.26, 0.26) for InSb; from the point (0.43, 0.43, 0.43) to the point (0.26, 0.26, 0.26) and from L to the point (0.30, 0.30, 0.30) for InAs and for the bands $V_1 \to C_1$ and $V_2 \to C_1$, respectively. A part of their intensity corresponds to the very small δ (AlSb) and 2δ vicinity (GaSb, InSb, and InAs) of the Λ axis on the ΓLK plane and a small area at the intersection of the ΓKWX and ΓLW planes near the points (0.14, 0.06, 0.0), (0.17, 0.09, 0.0), (0.20, 0.10, 0.0), and (0.23, 0.12, 0.0) for AlSb, GaSb, InSb, and InAs, respectively.

In contrast to the simplified results reported in [8–13, 17–19, 21], our data show that, for all four crystals, the localization of both bands of the transitions $V_1 \to C_1$ and $V_2 \to C_1$ along the $\Gamma - L$ direction is complex and inhomogeneous: they occur not only in the closest vicinity of the point L, but also in specific regions on the Λ axis (in contrast to [8–13, 18]) and the ΓLK plane (as in [10] for GaSb); the transitions from V_1 to V_2 along Λ have radically different intensi-

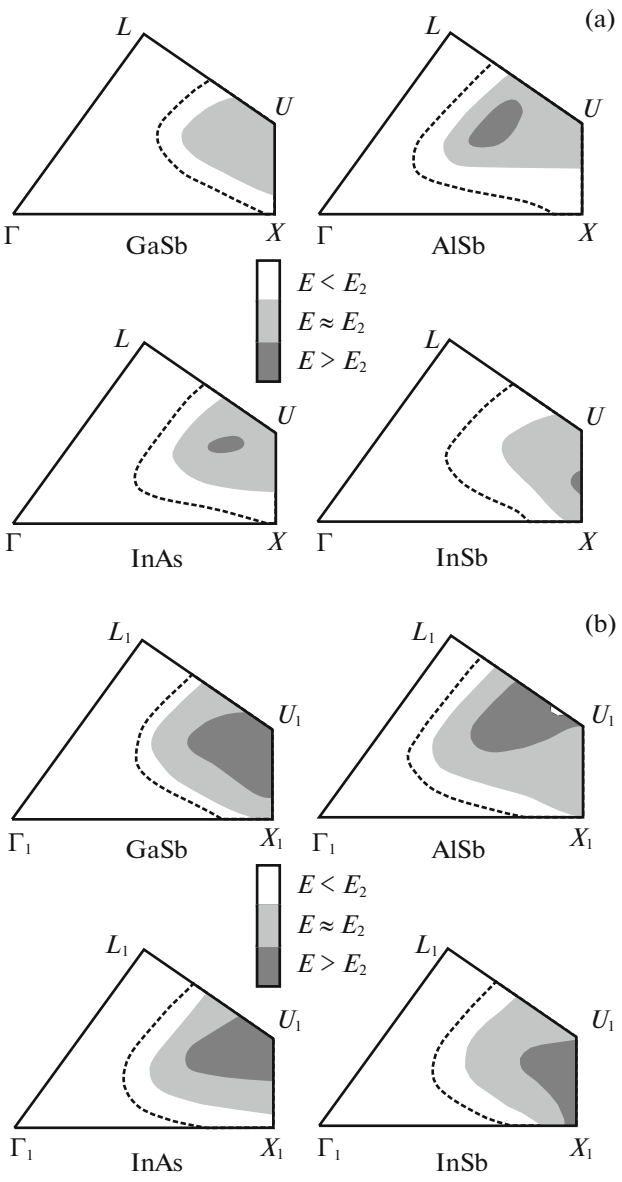

Fig. 3. Localization of the interband transitions for the main E_2 maximum of the AlSb, GaSb, InSb, and InAs crystals on (a) the Γ*LUX* and (b) $\Gamma_1L_1U_1X_1$ planes (region I).

ties, despite the degeneracy of this pair in energy; in the vicinity of the intersection of the Γ*KWX* and Γ*LW* planes, their intensities significantly increase.

3.2. The E_0' Step

In the case of the E_0' step, our data are more detailed than the results of other calculations. The most important role in all of the investigated compounds is played by the transitions $V_{1,2} \to C_2$ in the vicinity of ~(3–4)δ near the BZ center (on average, the transitions in AlSb are a bit closer to the point Γ than in InSb) and the transitions $V_{1,2} \to C_1$ along the segments on the Γ*KWX* plane near the Δ axis. In GaSb, InSb, and InAs, the key role is played by the maxima in the spectra of partial contributions of the transitions from the two UVBs to the second LCB and in AlSb the transitions from the second UVB to the LCB are most important.

3.3. The E_2 Maximum

The maximum of the most intense band is located at ~4.05 eV (AlSb), 4.23 eV (GaSb), 3.83 eV (InSb), and 4.54 eV (InAs) (Table 1 and Fig. 2). It is related by ~(88 ± 4)% to the transitions from the UVBs to the LCB in the large region of the bulk of the BZ (Table 2). The entire set of **k** points can be divided into the following regions: (i) the vicinity of the Γ*LUX* plane (region I in Fig. 3), (ii) the vicinity of the Γ*LK* plane (region II in Fig. 4), and (iii) the vicinity of the $\Gamma_2L_2U_2X_2$ plane (region III in Fig. 1). Since the band E_2 is relatively wide, regions I, II, and III are separated into an additional three parts responsible for (i) the long-wavelength (white) and (ii) short-wavelength (dark-grey) parts of the structure E_2 and (iii) the immediate vicinity of the maximum (light-grey). We limit the long-wavelength side of the main maximum by energies to 3.90 eV (AlSb), 4.16 eV (GaSb), 3.64 eV (InSb), and 4.27 eV (InAs) and the short-wavelength side, to 4.21 eV (AlSb), 4.30 eV (GaSb), 3.96 eV (InSb), and 4.76 eV (InAs).

The transitions concentrated in region I are responsible for ~(42–51)% of the contribution to the band E_2 and are limited in the BZ by the Γ*LUX* and $\Gamma_1L_1U_1X_1$ planes. The points Γ_1, L_1, U_1, and X_1 have the coordinates (δ, δ, 0.0), (0.5 + δ/3, 0.5 + δ/3, 0.5 – 2δ/3), (1.0, 0.25 + 0.5δ, 0.25–0.5δ), and (1.0, δ, 0.0), respectively. Thus, region I for all the crystals occupies a significant part on the Γ*LUX* ($\Gamma_1L_1U_1X_1$) face and is limited by the segments Γ–*X* (Γ_1–X_1), *X*–*U* (X_1–U_1), and *L*–*U* (L_1–U_1) on one side and by a V-shaped curve with ends located on the Γ–*X* (Γ_1–X_1) and *L*–*U* (L_1–U_1) axes on the other side. The formation of the long-wavelength side of the band E_2 occurs mainly near this V-shaped curve. The region located closer to the point *U* (U_1) and the *U*–*X* (U_1–X_1) axis is responsible for the short-wavelength side. Although the distance between the outer and inner faces of region I is very small (~$\delta/\sqrt{2}$), the configuration and intensity radically change upon transition from the first to the second face (Table 2): the region itself somewhat increases, but the intensity decreases by a factor of 2–3. It follows explicitly from these data that the points *X* [8, 9, 17, 21], (0.75, 0.25, 0.25), [13], and the axes Δ [11, 19] and *X*–*U* [9] amount only to a small part of the wide spectrum of **k** points responsible for the intense transitions at Γ*LUX* and $\Gamma_1L_1U_1X_1$.

The description of region II is similar to that of region I, if we replace the Γ*LUX* plane with the Γ*LK*

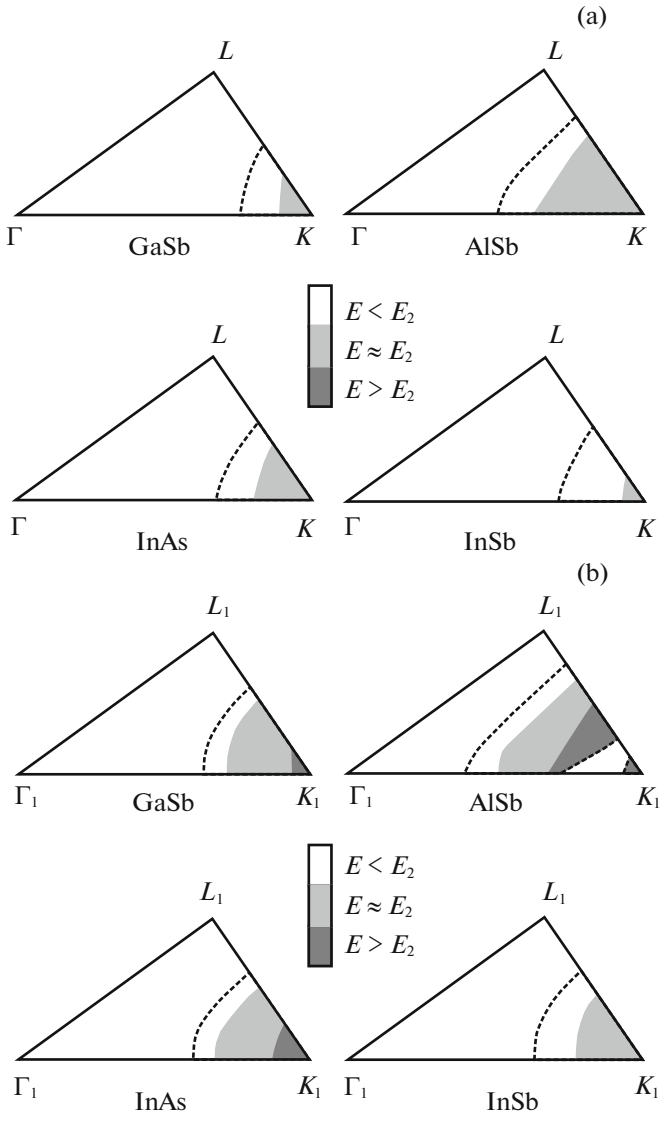

Fig. 4. Localization of the interband transitions for the main E_2 maximum of the AlSb, GaSb, InSb, and InAs crystals on (a) the ΓLK and (b) $\Gamma_1 L_1 K_1$ planes (region II).

one and the $\Gamma_1 L_1 U_1 X_1$ plane with the $\Gamma_1 L_1 K_1$ one (Fig. 4). The point K_1 has the coordinates (0.75 + 0.5δ, 0.75–0.5δ, 0). On the ΓLK face, the Σ axis, especially near the vertex K, is the most important for our investigations: in particular, in InSb its role is insignificant (~3%); in GaSb and InAs, its contribution is ~7%; and in AlSb, it is ~13%. Thus, the Σ-axis value is not as important in the formation of the band E_2 as was described in [8, 11, 12, 18, 19, 21].

Region III is located in the δ vicinity of the $\Gamma_2 L_2 U_2 X_2$ plane; its position in the irreducible part of the BZ is schematically shown in Fig. 1 along the B_1B_2 and B_1B_3 segments. For all four crystals, the point B_1 has the coordinates (0.85, 0.11, 0.0); the point B_2 has the coordinates (0.45, 0.225, 0.00) for AlSb and (0.5, 0.25, 0.0) for the remaining crystals; and the point B_3 has the coordinates (0.7, 0.5, 0.3) for InSb and (0.67, 0.5, 0.33) for the other crystals. The highest intensity of the transitions in region III is concentrated near the intersection of the ΓKWX and ΓLW planes, i.e., in the vicinity of the point B_2.

Thus, the band E_2 of the AlSb, GaSb, InSb, and InAs crystals is formed not in a narrow range of points, but in a wide region of **k** points located not only on the ΓLUX and ΓLK faces, as was mentioned in [10] for GaSb, but in the bulk of the BZ. The importance of the Δ and Σ axes depends heavily on the investigated compound.

3.4. The E_x Structure

The occurrence of the E_x structure following the E_2 structure in energy in the spectra of the theoretical $\varepsilon_2(E)$ curves is related to the occurrence of a weak maximum in transitions from the UVB to the second LCB at ~5.0 eV (AlSb, GaSb, InAs) and ~4.4 eV (InSb) (Table 1 and Fig. 2). They attain the highest intensity along the Δ axis from the point (0.43, 0.0, 0.0) to the point (0.78, 0.0, 0.0). In [9, 11, 13, 17] for GaSb, InSb, and InAs, these transitions occur from the point (0.50, 0.0, 0.0) to the point (0.7, 0.0, 0.0). The transitions of most interest occur in the bulk of the irreducible part of the BZ, which are not described in other publications. These transitions are less intense, than those located along the Δ axis and are concentrated along an arched curve. One end of this curve is located on the Λ axis at the points (0.33, 0.33, 0.33) for AlSb, (0.30, 0.30, 0.30) for GaSb, (0.26, 0.26, 0.26) for InSb, and (0.19, 0.19, 0.19) for InAs and the other end is located in the vicinity of the point (0.50, 0.28, 0.0) for GaSb, InSb, and InAs and the point (0.50, 0.25, 0.0) for AlSb.

3.5. The E_1' Maximum

The E_1' maximum is formed by the same pair of bands as E_x. This pair of bands is located in a wide spectrum of **k** points from the vicinity of the vertex L, but, in contrast to [9, 10, 13, 21] for GaSb, InSb, and InAs, there are no transitions at the point L itself. A part of the transitions is concentrated at the high-symmetry axes of the BZ; at the Λ axis in the vicinity of the points (0.45, 0.45, 0.45) for AlSb and GaSb (0.43, 0.43, 0.43) for InSb, and (0.37, 0.37, 0.37) for InAs; on the $L-U$ axis in the vicinity of the points (0.58, 0.46, 0.46) for AlSb, (0.56, 0.47, 0.47) for GaSb, (0.59, 0.455, 0.455) for InSb, and (0.61, 0.455, 0.445) for InAs; on the $L-K$ axis in the vicinity of the points located at the same distance from L as the points on the $L-U$ axis; and on the $L-W$ axis in the vicinity of the point (0.60, 0.50, 0.40) for all four crystals. In other studies, the transitions on the Λ axis for AlSb,

InSb, and InAs are located in the vicinity of the point (0.375, 0.375, 0.375) [11, 12]. Localization of the transitions on the $L-W$ axis was described only in [18] for GaSb, but without specifying a region. Transitions on the Δ axis, as in [11, 18] for GaSb, InSb, and InAs, were also revealed by us, but their intensity is very low.

4. CONCLUSIONS

The imaginary part of the permittivities of AlSb, GaSb, InSb, and InAs was calculated using the FP–LAPW technique in the generalized gradient approximation (GGA–PBE) in the range to ~7 eV. The novelty of this study is that, for III–V crystals, the most intense transitions can be concentrated not only in the vicinity of the high-symmetry axes of the Brillouin zone, but also in its bulk. This concerns, to the greatest extent, band E_2, which is formed with the involvement of a significant part of the Brillouin zone in the vicinity of the ΓLUX and ΓLK planes and in the vicinity of the point (0.45, 0.225, 0.0) for AlSb or (0.5, 0.25, 0.0) for GaSb, InSb, and InAs. Detailed schemes of localization of different parts of the transition bands in the bulk of the Brillouin zone are presented.

ACKNOWLEDGMENTS

We are grateful to A.I. Kalugin for his help with the calculations.

This study was supported by the Russian Foundation for Basic Research, project nos. 11-02-07038 and 12-02-07007.

REFERENCES

1. O. Ueda and S. J. Pearton, *Materials and Reliability Handbook for Semiconductor Optical and Electron Devices* (Springer, New York, 2013); Ch. Liu, Y. Li, and Y. Zeng, Engineering **2**, 617 (2010).
2. *Semiconductors and Semimetals*, Vol. 3: *Optical Properties of Semiconductors (Semiconductor Compounds of III–V Type),* Ed. by R. K. Willardson and A. C. Beer (Academic, New York, 1966).
3. V. V. Sobolev, *Optical Fundamental Spectra of III–V Compounds* (Shtiintsa, Kishinev, 1979) [in Russian].
4. P. Yu and M. Cardona, *Fundamentals of Semiconductors* (Springer, Berlin, 2005).
5. V. V. Sobolev, *Optical Properties and Electronic Structure of Nonmetals*, Vol. 1: *Introduction to the Theory* (Inst. Komp. Issled., Moscow, Izhevsk, 2012) [in Russian].
6. V. V. Sobolev, *Optical Properties and Electronic Structure of Nonmetals*, Vol. 2: *Simulation of Integral Spectra by Elementary Bands* (Inst. Komp. Issled., Moscow, Izhevsk, 2012) [in Russian].
7. V. V. Sobolev and V. V. Nemoshkalenko, *Electronic. Structure of Solids in the Region of Fundamental Absorption Edge*, Vol. 1: *Introduction to the Theory* (Naukova Dumka, Kiev, 1992) [in Russian].
8. F. H. Pollak, C. W. Higginbotham, and M. Cardona, in *Proceedings of the International Conference on Physics of Semiconductors* (Kyoto, Japan, 1966), Vol. 21, p. 20.
9. C. W. Higginbotham, F. H. Pollak, and M. Cardona, in *Proceedings of the 9 International Conference on Physics of Semiconductors* (Moscow, 1968), Vol. 11, p. 57.
10. R. N. Cahn and M. Cohen, Phys. Rev. B **1**, 2569 (1970).
11. V. C. De Alvarez, J. P. Walter, R. W. Boyd, and M. L. Cohen, J. Phys. Chem. Solids **34**, 337 (1973).
12. I. Topol, H. Neumann, and E. Hess, Czech. J. Phys. B **24**, 107 (1974).
13. J. R. Chelikowsky and M. L. Cohen, Phys. Rev. B **14**, 556 (1976).
14. M. Alouani, L. Brey, and N. E. Christensen, Phys. Rev. B **37**, 1167 (1988).
15. M.-Zh. Huang and W. Y. Ching, Phys. Rev. B **47**, 9449 (1993).
16. R. Asahi, W. Mannstadt, and A. J. Freeman, Phys. Rev. B **59**, 7486 (1999).
17. S. H. Rhim, M. Kim, A. J. Freeman, and R. Asahi, Phys. Rev. B **71**, 045202 (2005).
18. A. H. Reshak, Eur. Phys. J. B **47**, 503 (2005).
19. Zh. Feng, H. Hu, Sh. Cui, W. Wang, and C. Lu, Centr. Eur. J. Phys. **7**, 786 (2009).
20. N. N. Anua, R. Ahmed, A. Shaari, M. A. Saeed, B. U. Haq, and S. Goumri-Said, Semicond. Sci. Technol. **28**, 105015 (2013).
21. M. I. Ziane, Z. Bensaad, B. Labdelli, and H. Bennacer, Sens. Transducer. **27**, 374 (2014).
22. Y. Wang, H. Yin, R. Cao, F. Zahid, Y. Zhu, L. Liu, J. Wang, and H. Guo, Phys. Rev. B **87**, 235203 (2013).
23. B. D. Malone and M. L. Cohen, J. Phys.: Condens. Matter **25**, 105503 (2013).
24. S. Zollner, Ch. Lin, E. Schönherr, A. Böhringer, and M. Cardona, J. Appl. Phys. **66**, 383 (1989).
25. S. Zollner, M. Garriga, J. Humlicek, S. Gopalan, and M. Cardona, Phys. Rev. B **43**, 4349 (1991).
26. S. Logothetidis, L. Viña, and M. Cardona, Phys. Rev. B **31**, 947 (1985).
27. T. J. Kim, J. J. Yoon, S. Y. Hwang, Y. W. Jung, T. H. Chong, Y. D. Kim, H. Kim, and Y.-Ch. Chang, Appl. Phys. Lett. **97**, 171912 (2010).
28. *Springer Handbook of Condensed Matter and Materials Data*, Ed. by W. Martienssen and H. Warlimont (Springer, Berlin, 2005).
29. A. V. Bakulin and S. E. Kul'kova, Russ. Phys. J. **57**, 996 (2014).
30. P. Blaha, K. Schwarz, G. K. H. Madsen, D. Kvasnicka, and J. Luitz, *WIEN2K* (Techn. Univ. Wien, Austria, 2001).
31. J. P. Perdew, S. Burke, and M. Ernzerhof, Phys. Rev. Lett. **77**, 3865 (1996).
32. P. E. Blöchl, O. Jepsen, and O. K. Andersen, Phys. Rev. B **49**, 16223 (1994).
33. R. Markowski and M. Podgorny, J. Phys.: Condens. Matter **3**, 9041 (1991).

Translated by E. Bondareva